

Electronic Supplementary Information

A Wearable, Minimally-Invasive, Fully Electrochemically-Controlled Feedback Minisystem for Diabetes Management

Yiqun Liu,^a Qi Yu,^b Le Ye,^c Li Yang,^{*b} Yue Cui^{*a}

^aSchool of Materials Science and Engineering, Peking University; First Hospital Interdisciplinary Research Center, Peking University, Beijing 100871, P.R. China. Email: ycui@pku.edu.cn

^bRenal Division, Peking University First Hospital; Peking University Institute of Nephrology; Key Laboratory of Renal Dis-ease, Ministry of Health of China; Key Laboratory of Chronic Kidney Disease Prevention and Treatment (Peking University), Ministry of Education, Beijing, 100034, P.R. China. Email: li.yang@bjmu.edu.cn

^cInstitute of Microelectronics, Peking University, Beijing 100871, P.R. China.

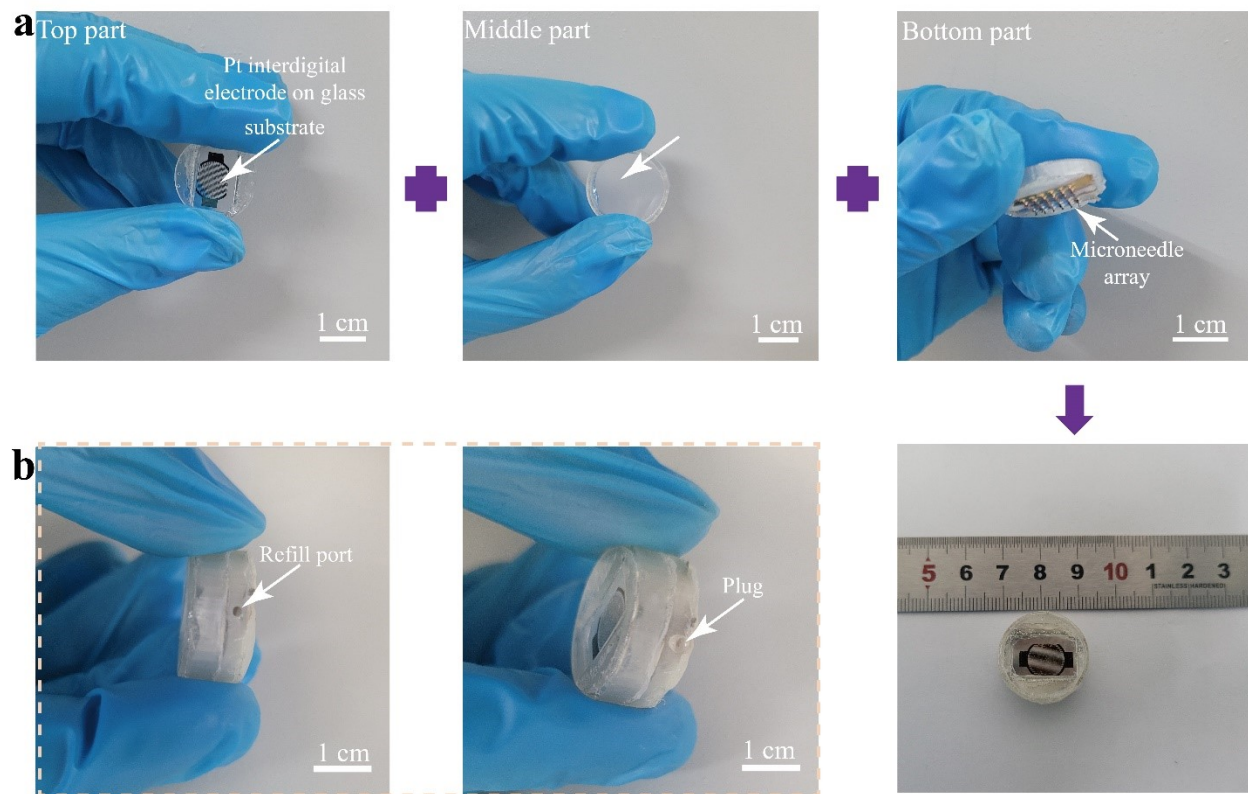


Fig. S1 Components of the system. (a) Camera images of different components of the system. (b) Camera images of the refill port and plug in the system.

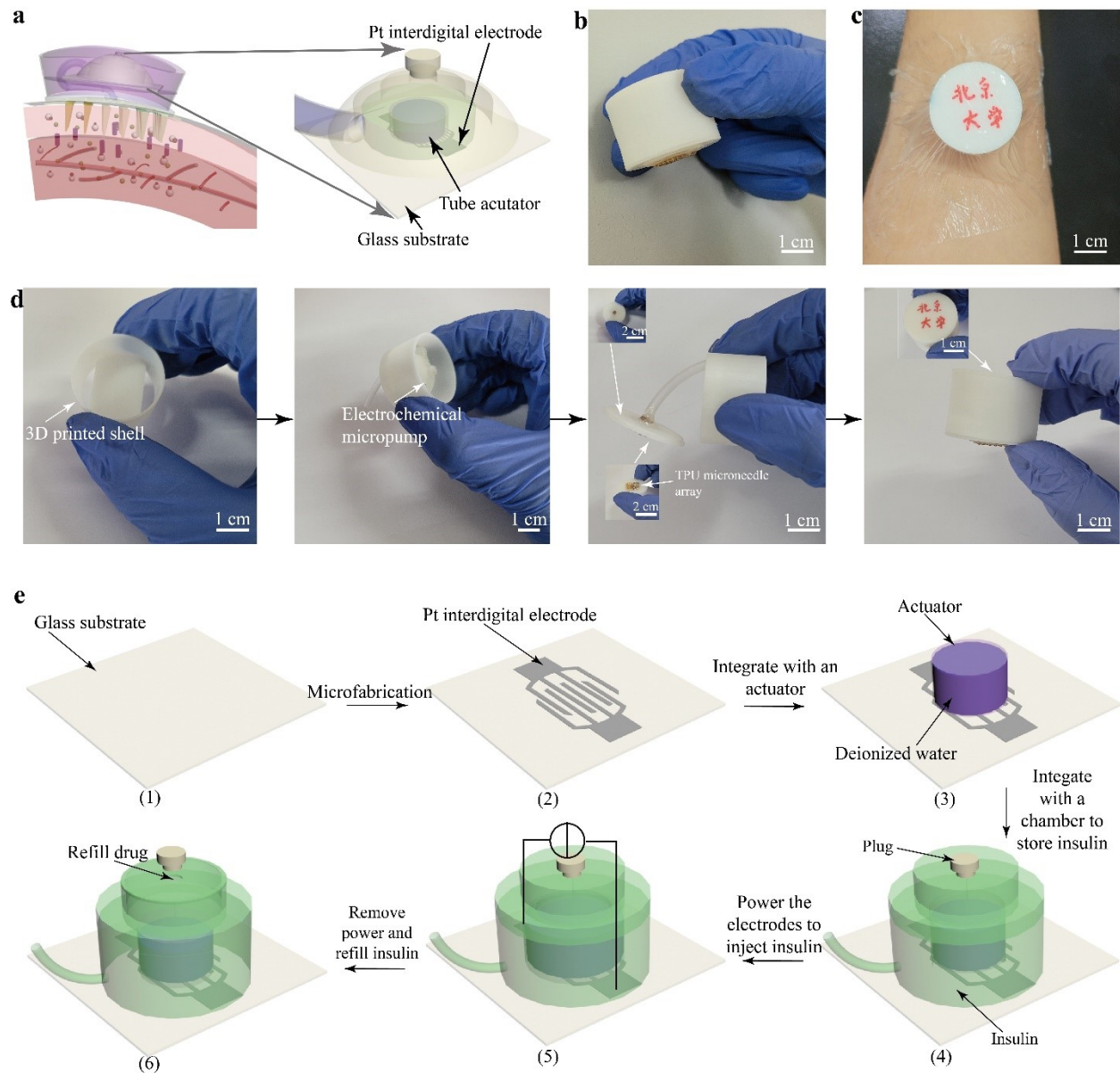


Fig. S2 Another form of the electrochemical micropump to form the closed-loop system with a larger size for storing more insulin solution. (a) Illustrative scheme of another form of the electrochemical micropump to form the closed-loop system. (b) Photograph of the whole system. (c) Photograph of the system applied to the arm of the human body. (d) The assemble and package process of the biosensor and micropump. (e) Fabrication process of the micropump.

The working principle of this micropump (in Fig. S2) was same as that shown in Fig. 1a. The actuator was in a cylinder made of commercially available Teflon membrane (30 μm thick) that was adhered and sealed to the Pt interdigital electrodes with a waterproof adhesive. The cylinder had a diameter of about 7 mm and a height of about 7 mm, and was filled with deionized water as the electrolyte. The actuator and electrodes were then encapsulated in a 3D printed hollow chamber with a bottom diameter of 2.3 cm and a height of 1 cm. The micropump was integrated with the TPU microneedles and a flexible catheter for controlling the release of insulin into the dermis through the internal channels of the hollow microneedle. Finally, the micropump and the microneedle arrays were packaged in a 3D printed cylinder (3 cm in diameter and 2 cm in height).

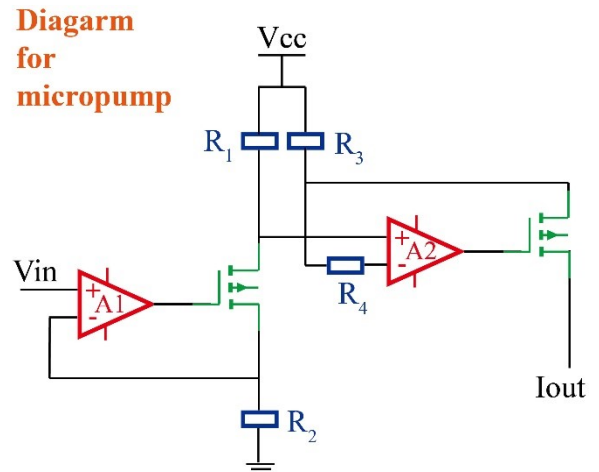
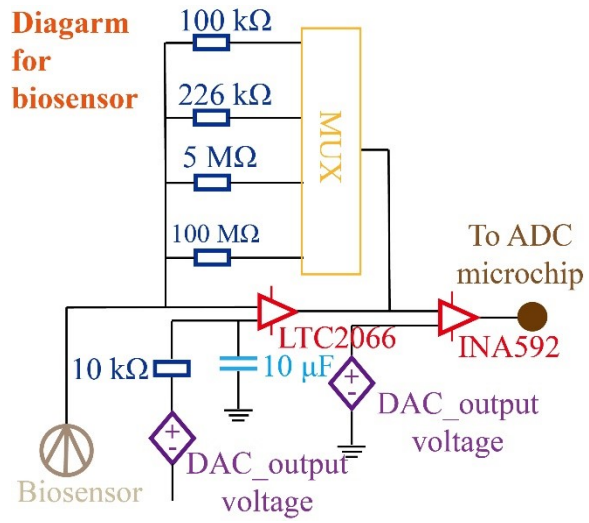


Fig. S3 Schematic diagram of PCB for the biosensor and micropump.

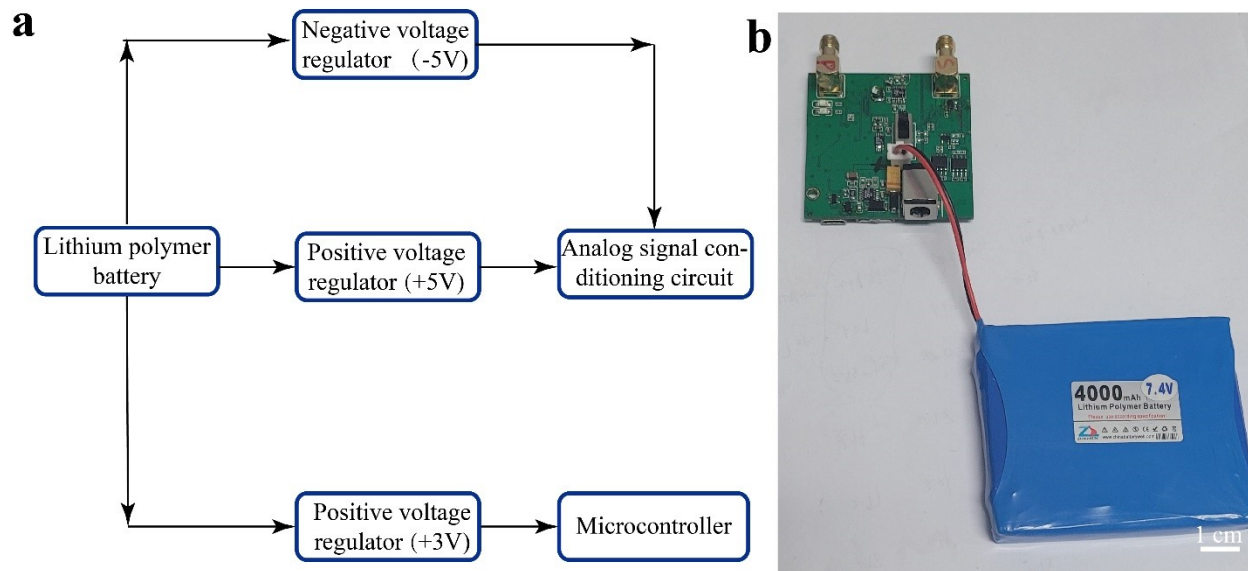


Fig. S4 Power delivery and battery for the system. (a) Power delivery diagram of the system. (b) The representative photograph of the battery module used in the current work.

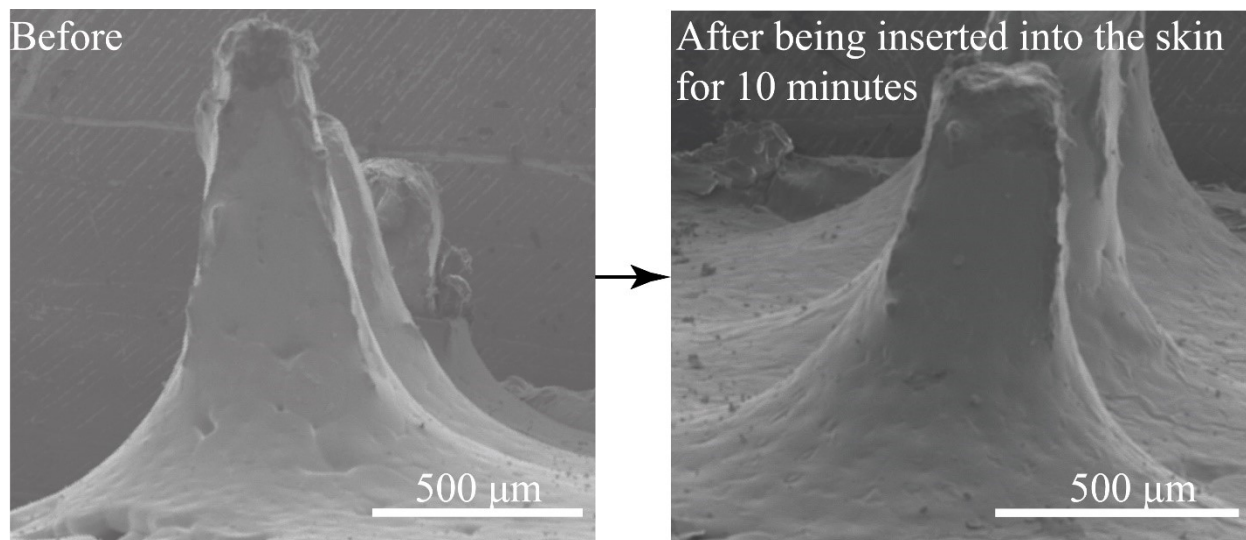


Fig. S5 SEM images of the microneedle before and after being inserted into the skin for 10 min.

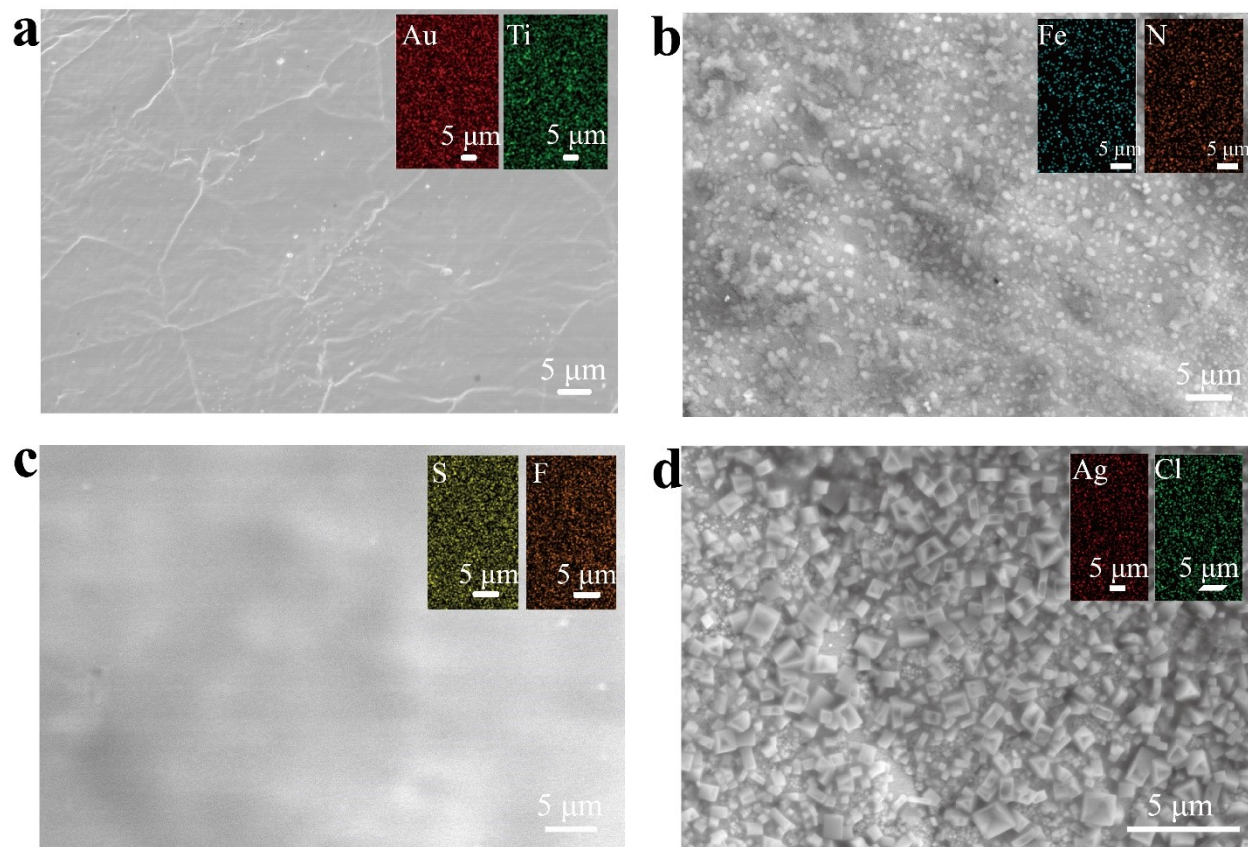


Fig. S6 SEM images and EDS mapping analysis of the Au electrode and the Ag/AgCl electrode. (a) The original Au electrode. (b) The Au electrode after the deposition of Prussian blue. (c) The Au electrode modified with the Nafion membrane. (d) The Ag/AgCl electrode.

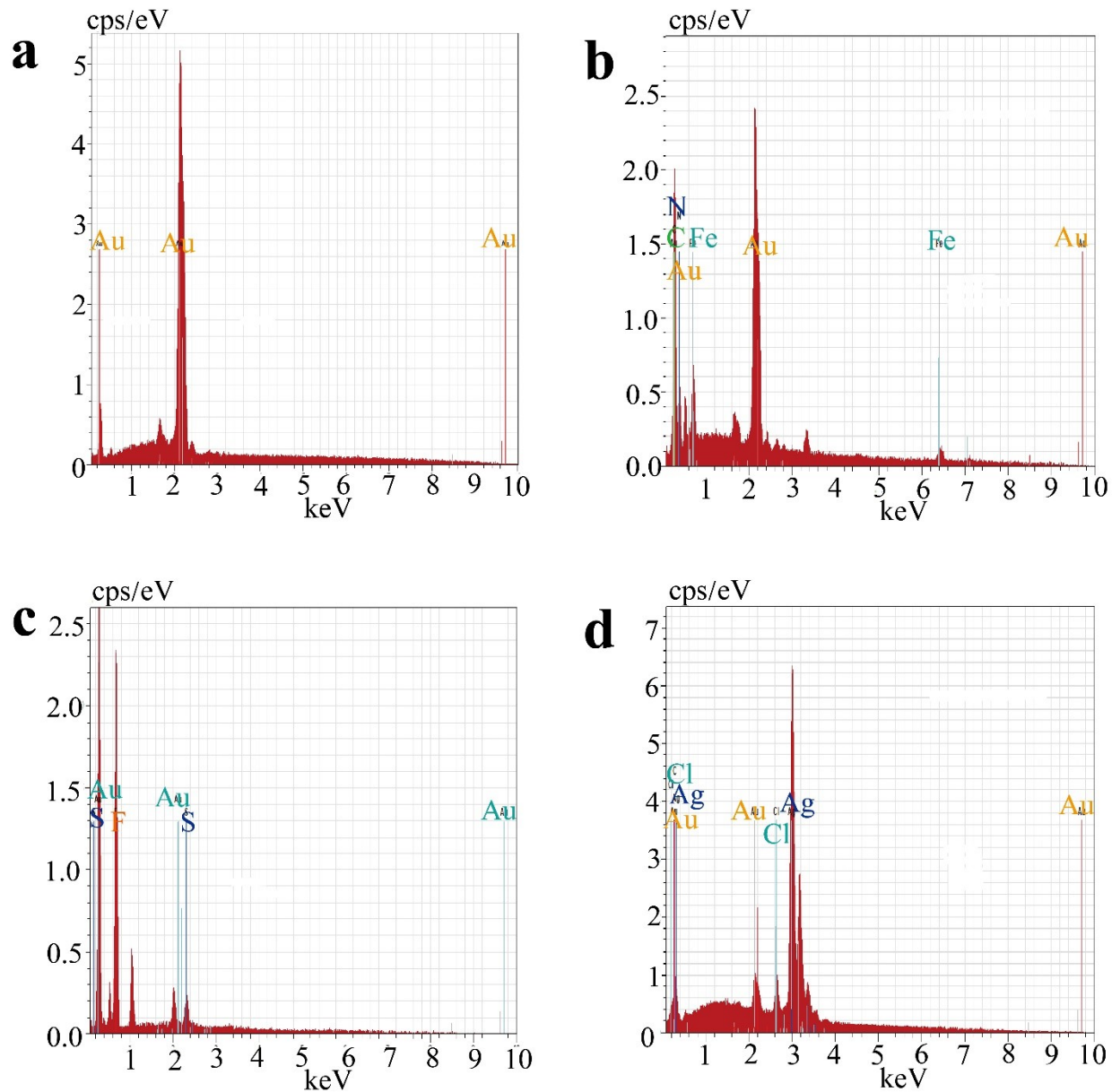


Fig. S7 EDS point analysis of the Au electrode and the Ag/AgCl electrode. (a) The original Au electrode. (b) The Au electrode after the deposition of Prussian blue. (c) The Au electrode modified with the Nafion membrane. (d) The Ag/AgCl electrode.

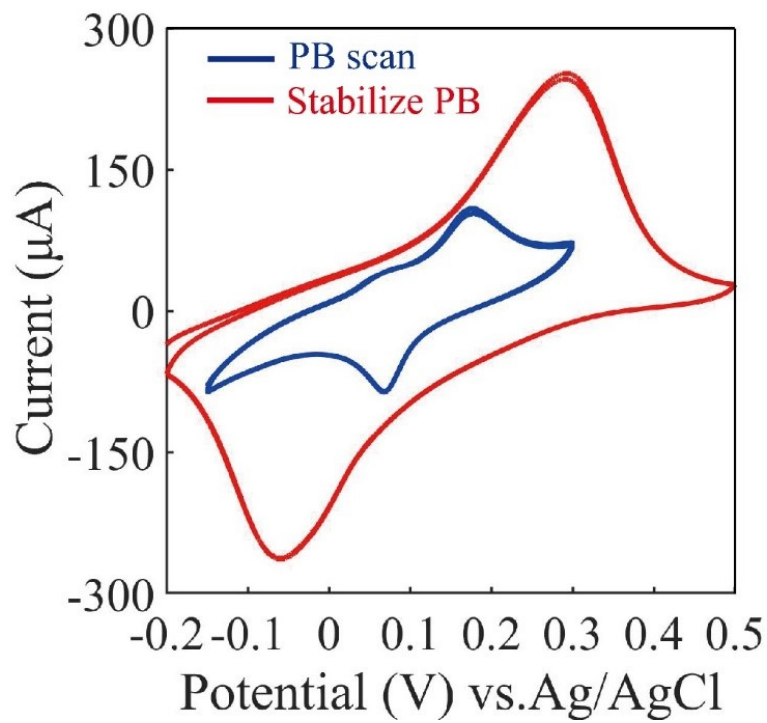


Fig. S8 Cyclic voltammograms for electrodepositing and stabilizing Prussian blue layer on the Au electrode.

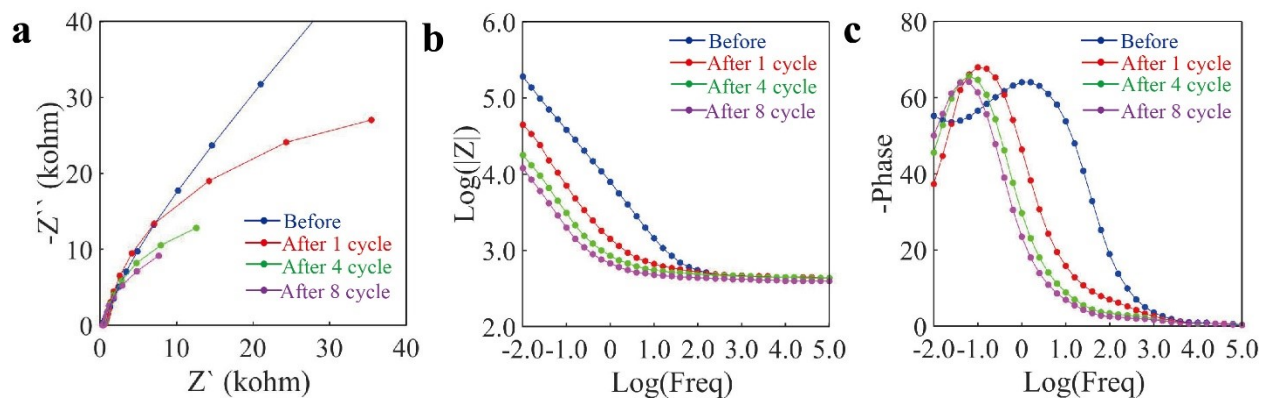


Fig. S9 Nyquist and Bode plots of the Au working electrode after the deposition of different cycles of Prussian blue in the scan frequency from 1×10^{-2} to 1×10^5 Hz. (a) Magnified image of the Nyquist plot in low impedance. (a) Bode plot of impedance. (b) Bode plot of phase.

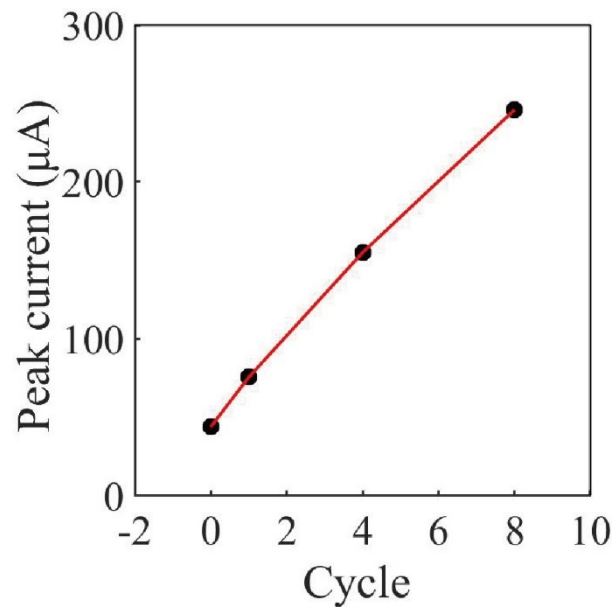


Fig. S10 The oxidation peak currents of cyclic voltammograms of the biosensor with different thicknesses of PB layer in the 0.1 M KCl/HCl solution.

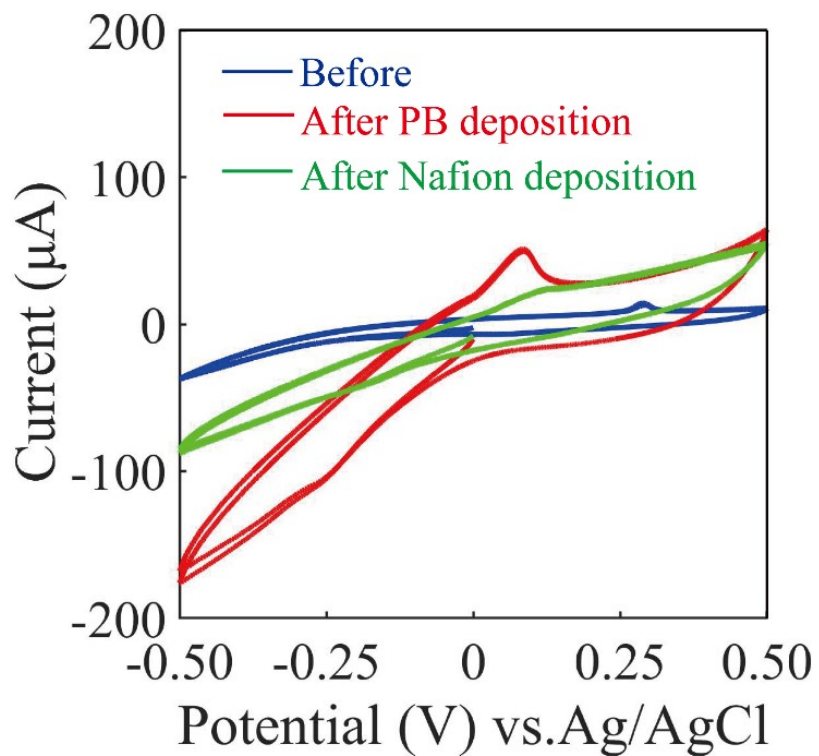


Fig. S11 The cyclic voltammograms of the biosensor before and after the deposition of Prussian blue, and Nafion membrane in PBS containing 4 mM H_2O_2 (scanning rate: 100 mV/s).

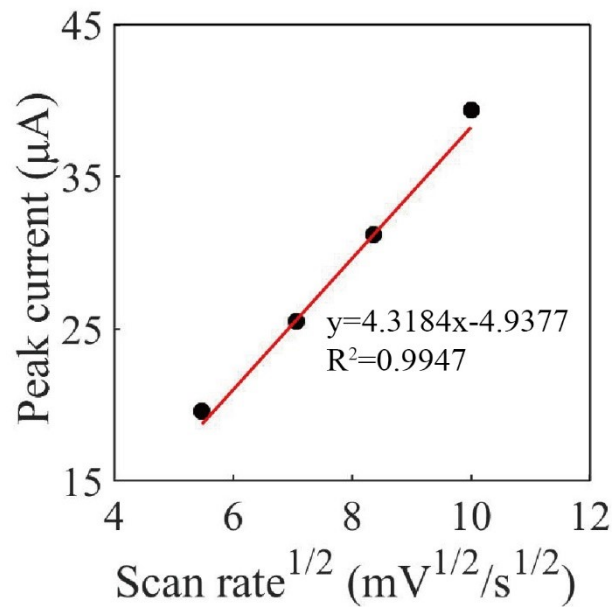


Fig. S12 Relationship between peak currents and the square root of scan rates in the cyclic voltammograms curves of the biosensor for sensing 4 mM H₂O₂ in PBS at different scan rates.

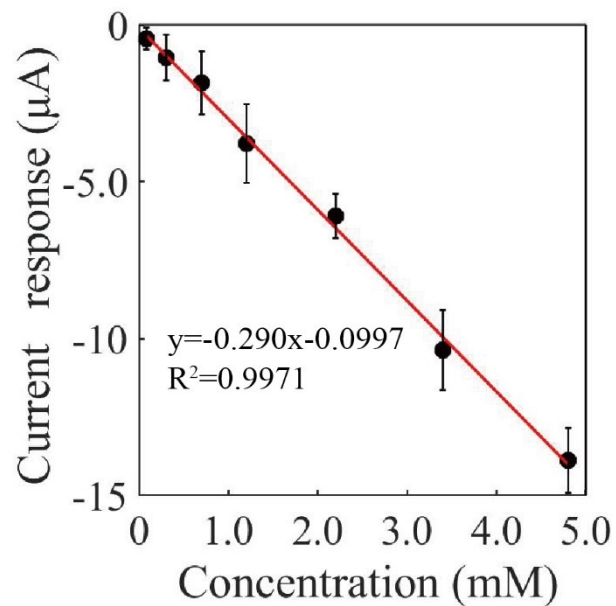


Fig. S13 Calibration curve upon the additions of H_2O_2 in PBS on the biosensor ($n=3$). Relationship between peak currents and the square root of scan rates in the cyclic voltammograms curves of the biosensor for sensing 4 mM H_2O_2 in PBS at different scan rates.

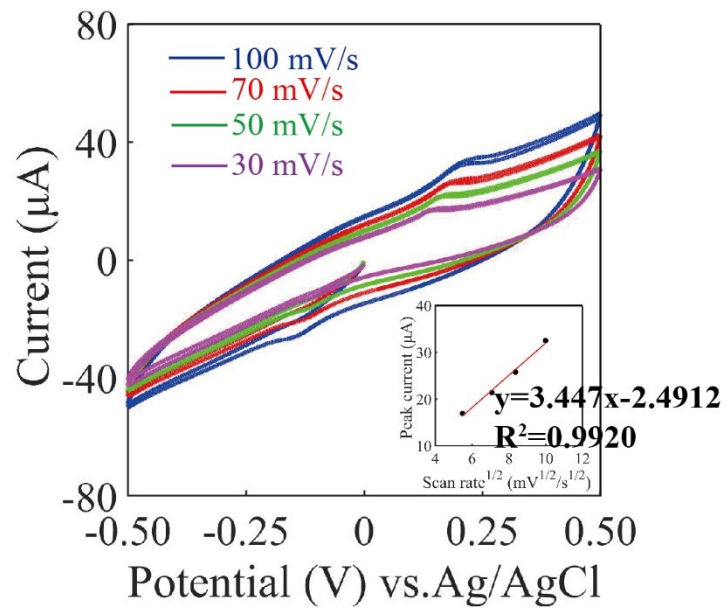


Fig. S14 The cyclic voltammograms and calibration curve of the biosensor for sensing 4 mM glucose in PBS at different scan rates.

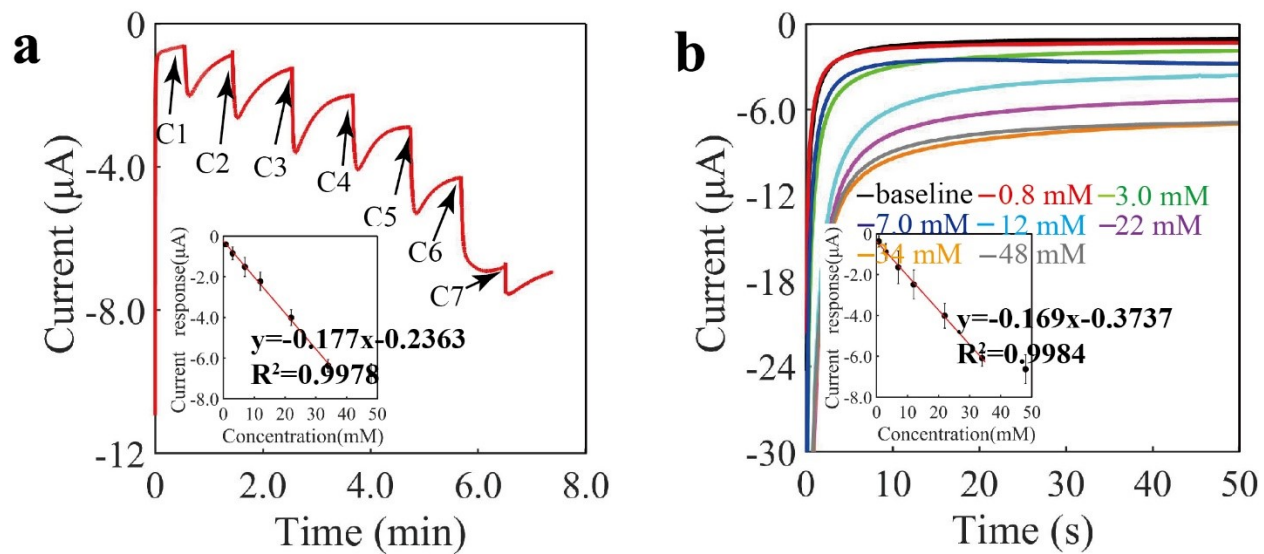


Fig. S15 Performance of the biosensor for sensing 4 mM glucose in PBS at different scan rates. (a) The current-verses-time response and calibration curve for detecting glucose in PBS (n=3). C1: 0.8 mM, C2: 2.2 mM, C3: 4.0 mM, C4: 5.0 mM, C5: 10 mM, C6: 12 mM, C7: 14 mM. (b) Current baseline response and calibration curve for detecting glucose in PBS (n=3).

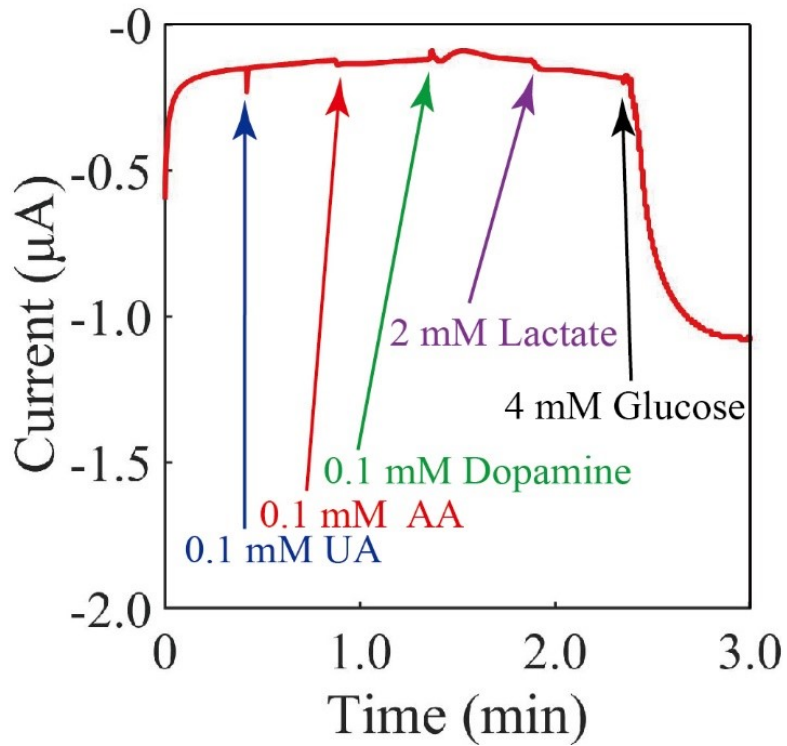


Fig. S16 The selective response of the sensor to glucose and other interfering substances (UA: uric acid, AA: ascorbic acid).

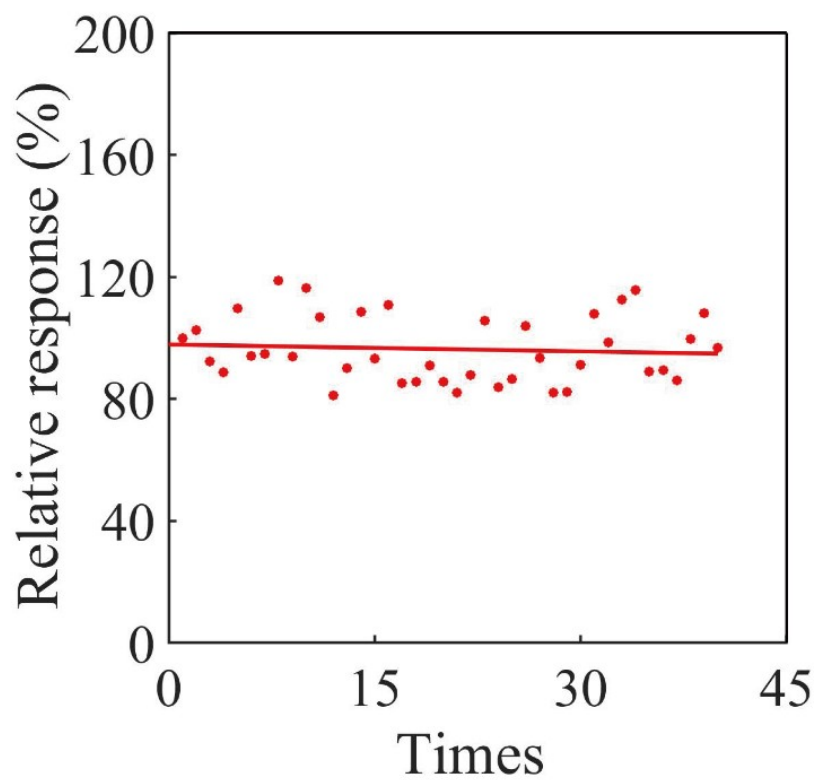


Fig. S17 Repeatability study of the biosensor. The repeatability study was conducted by continuously measuring the glucose for 40 times.

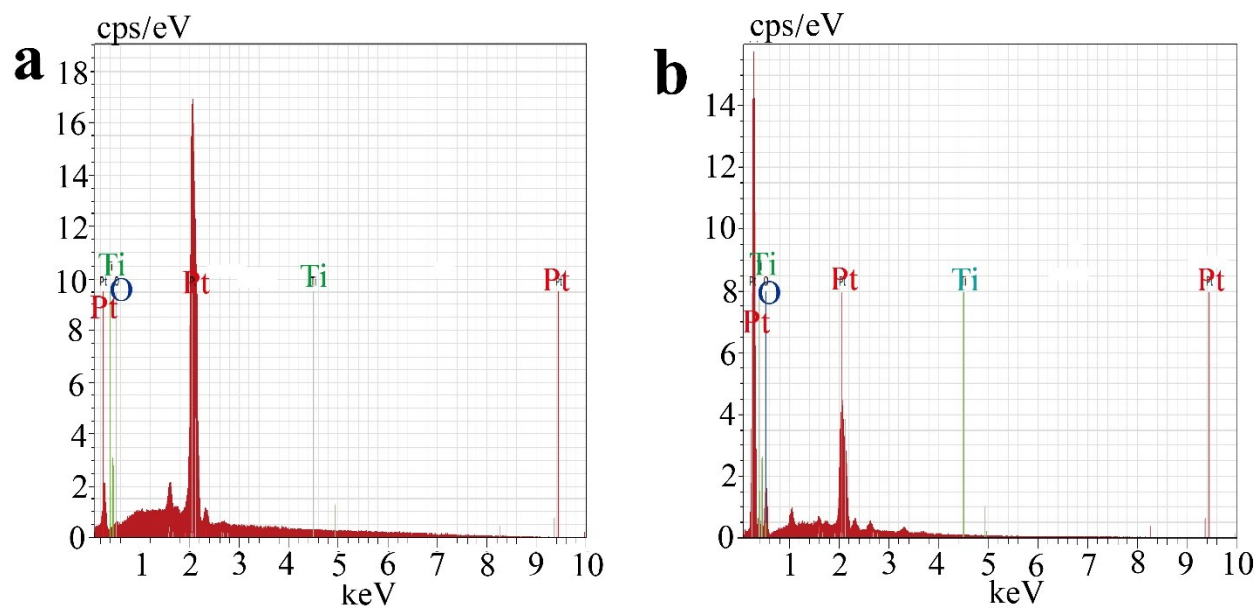


Fig. S18 EDS point analysis of the Pt interdigital electrode. (a) The original Pt interdigital electrode. (b) The Pt interdigital electrode after oxidation and degradation.

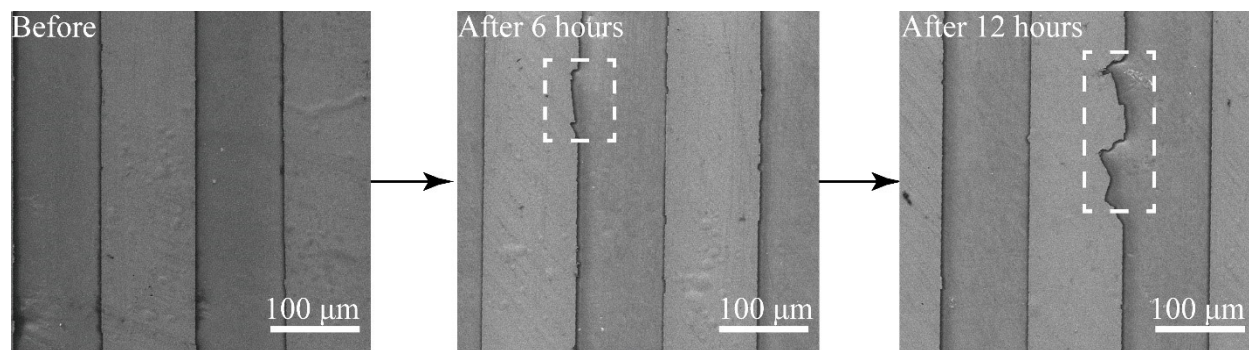


Fig. S19 SEM images of the original Pt interdigital electrode and after continuous working in 2 mA for 6 and 12 hrs.

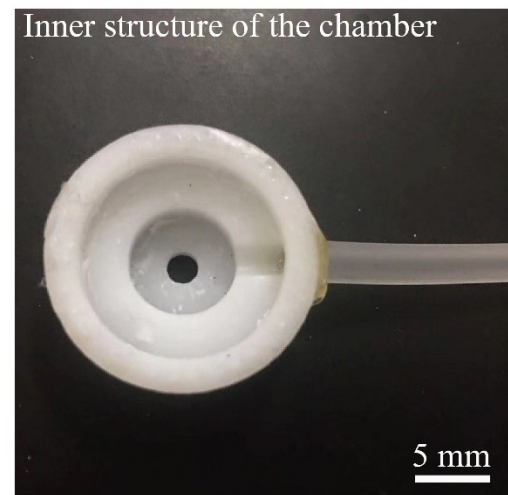
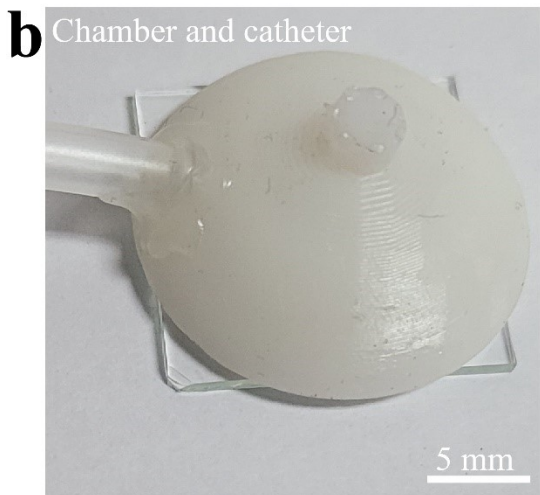
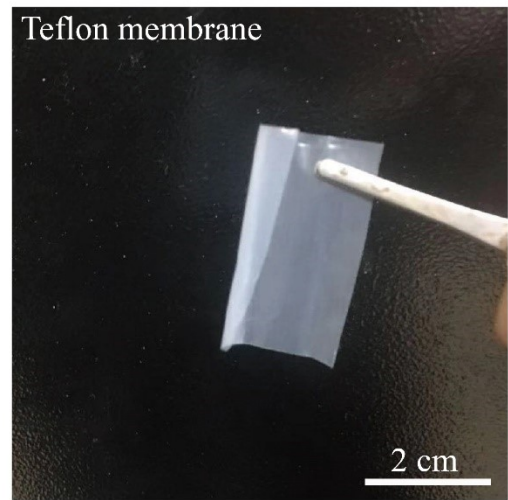
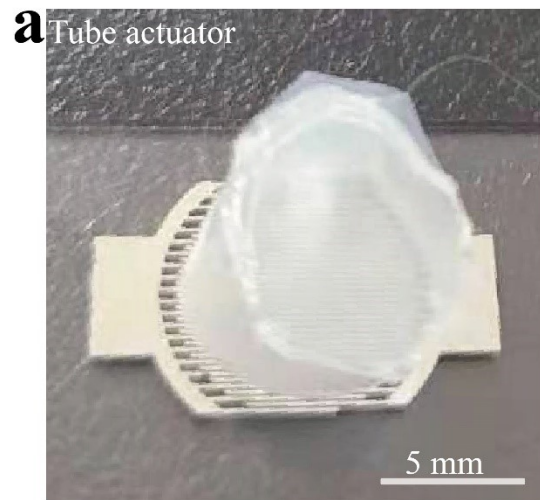


Fig. S20 Camera images of the actuator and the Teflon membrane (a), the chamber and catheter (b).

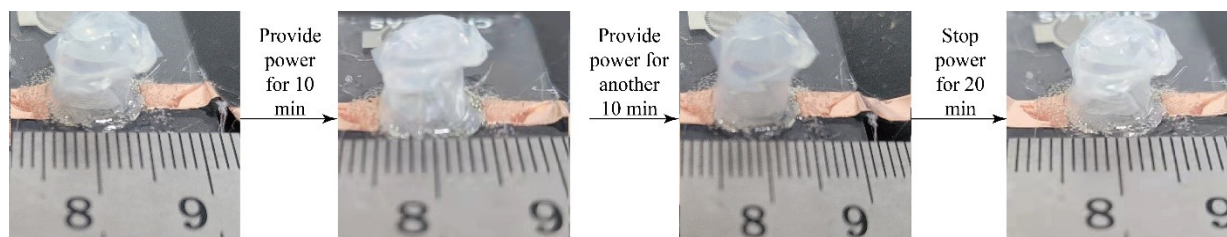


Fig. S21 Photographs of the shape change of the actuator under 1 mA in 20 minutes and after stopping the power for 20 min.

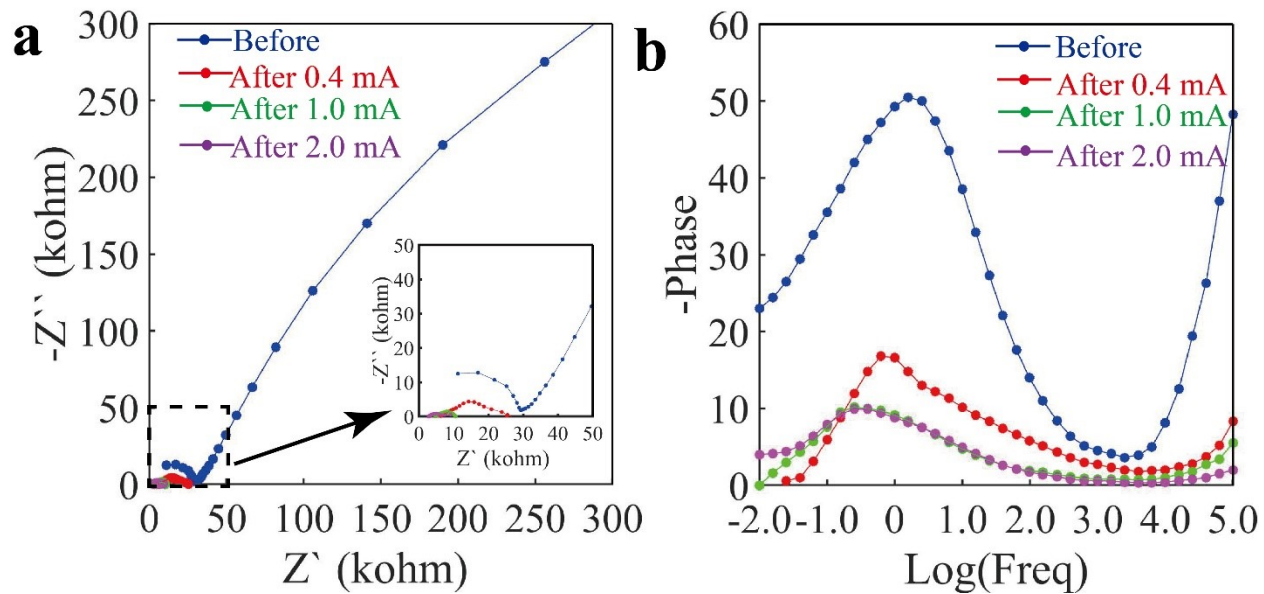


Fig. S22 Nyquist and Bode plot of the Pt interdigital electrode after the application of different constant currents for 10 minutes in scan frequency from 1×10^{-2} to 1×10^5 Hz. (a) Nyquist plot. (b) Phase of Bode plot.

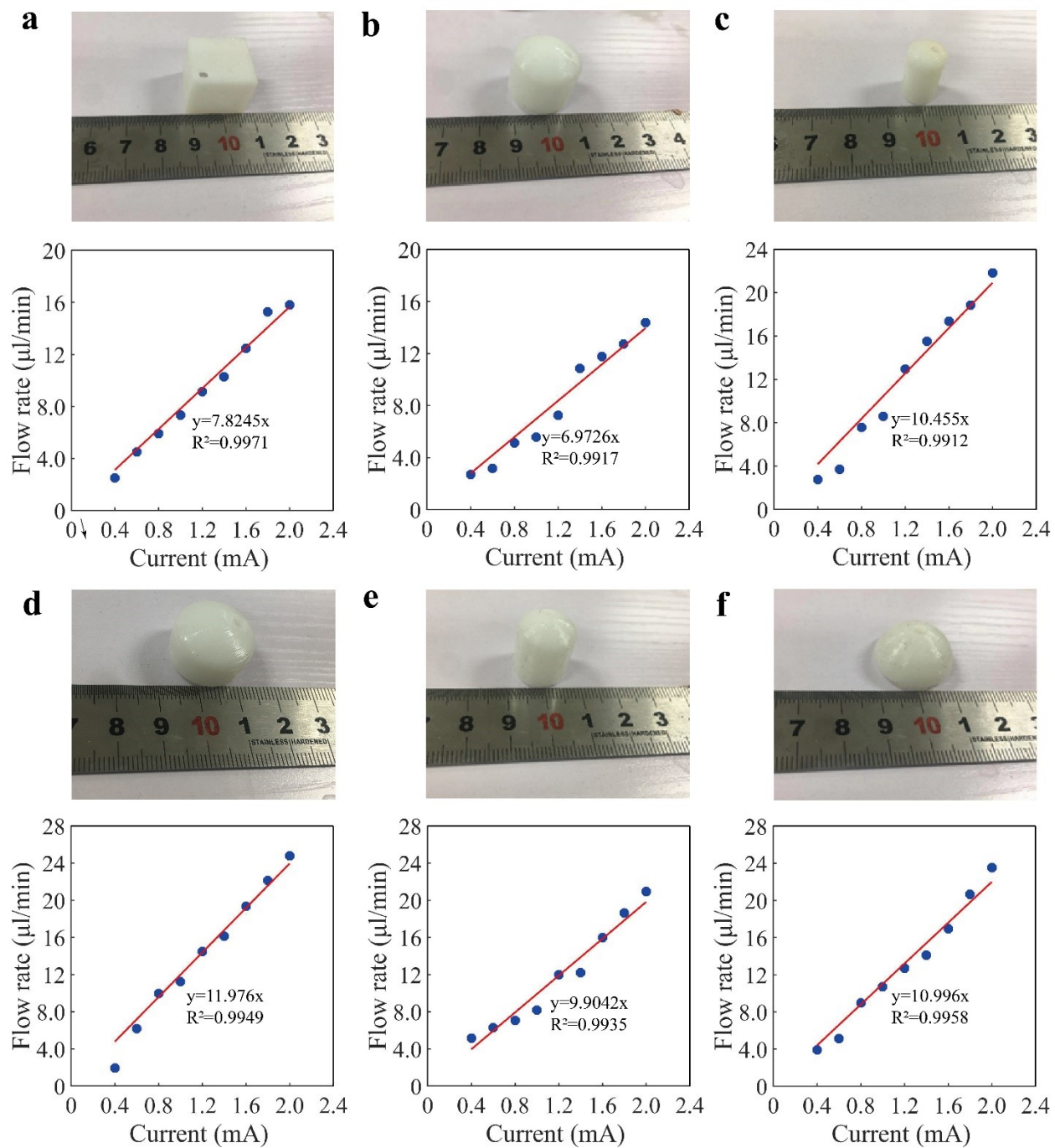


Fig. S23 Flow rate of the refillable electrochemical micropump with different shapes and sizes of the chamber.

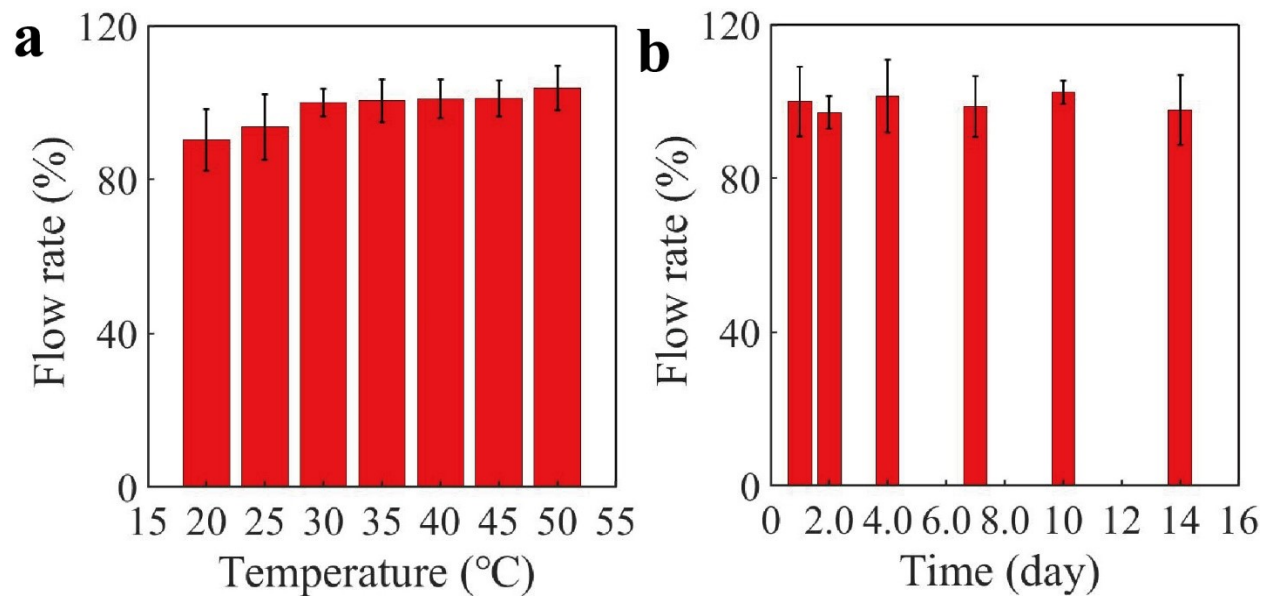


Fig. S24 Stability of the refillable electrochemical micropump. (a) The temperature stability of the micropump at 20 to 50 °C (n=3). (i) The storage stability of the sensor over 14 days (n=3).

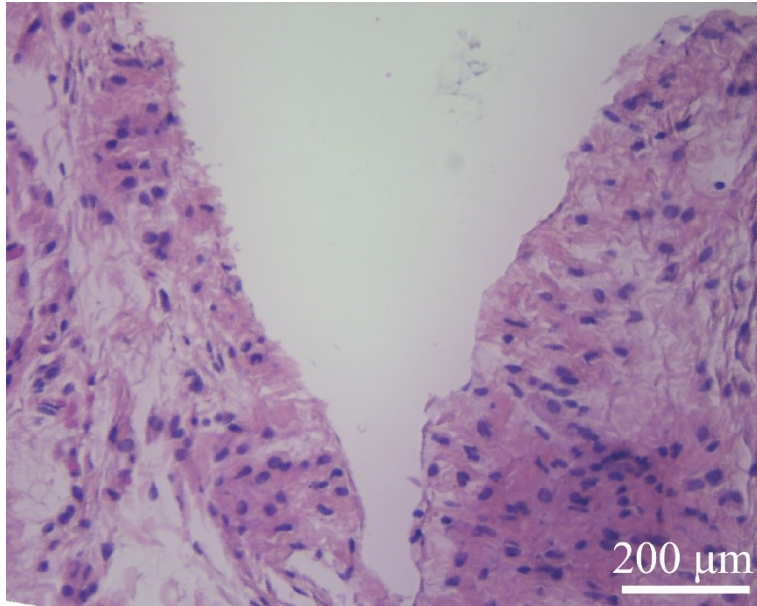


Fig. S25 An optical image of the hematoxylin and eosin-stained pierced skin section after removing the microneedle array.

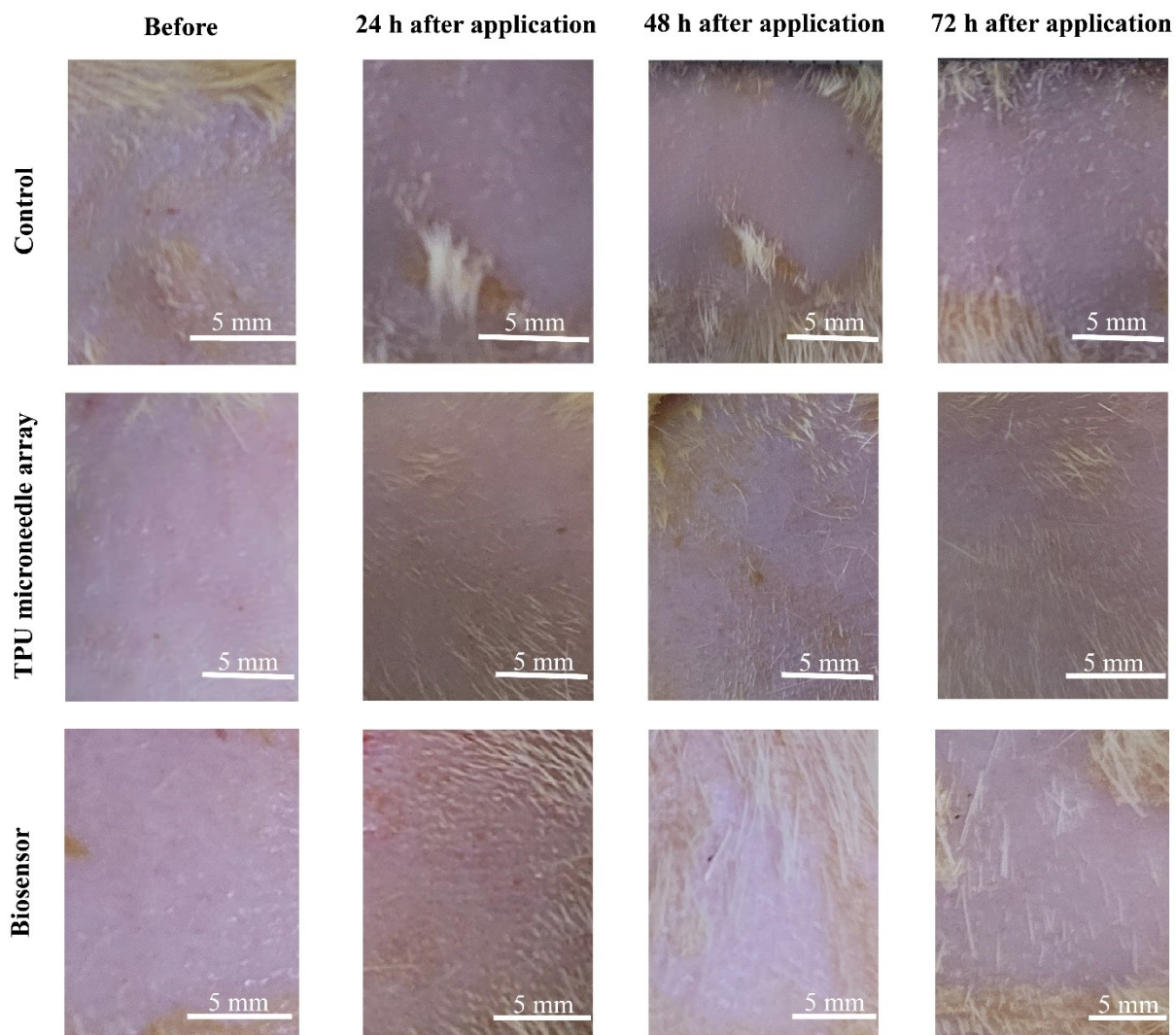


Fig. S26 Camera images of the rats' skin irritation test before and after removing the TPU microneedle array biosensor.

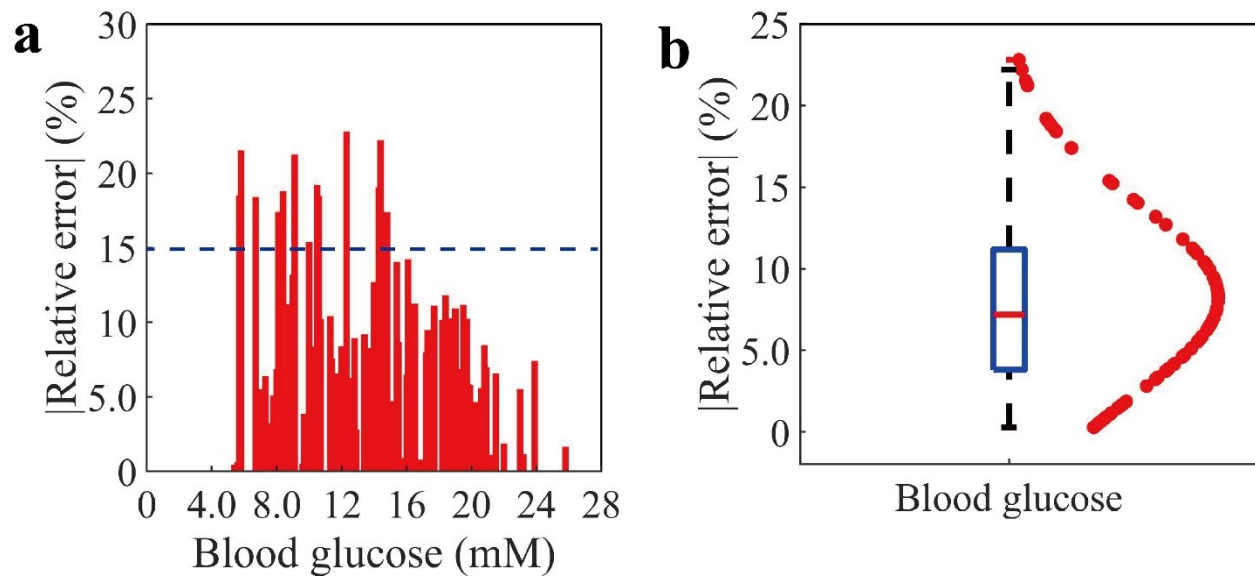


Fig. S27 Relative error of the biosensor at different blood glucose values (the data was from six diabetic rats).

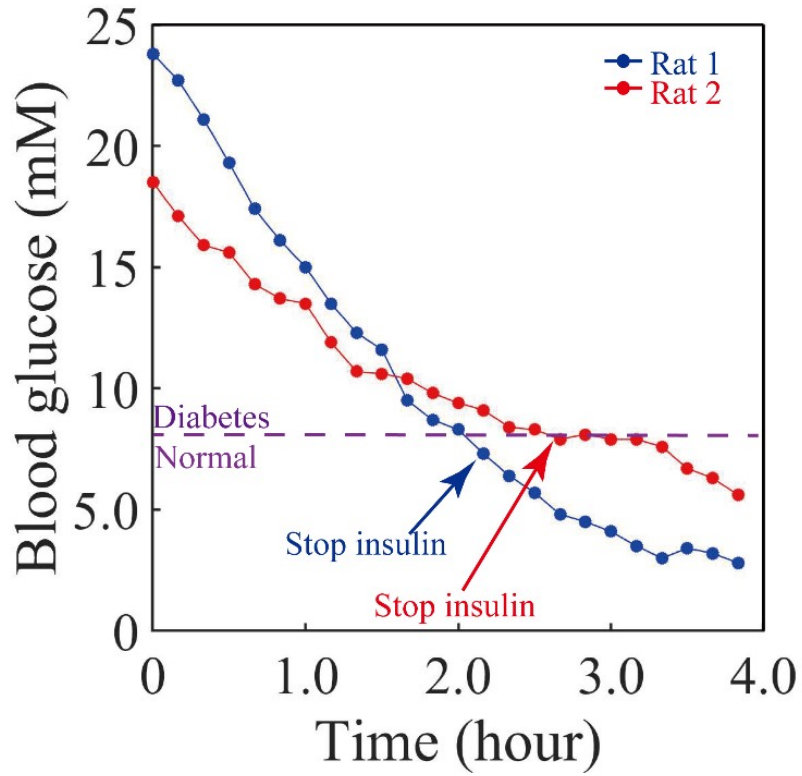


Fig. S28 The blood glucose levels versus time with the closed-loop button-like system in another two rats without a glucose intake.

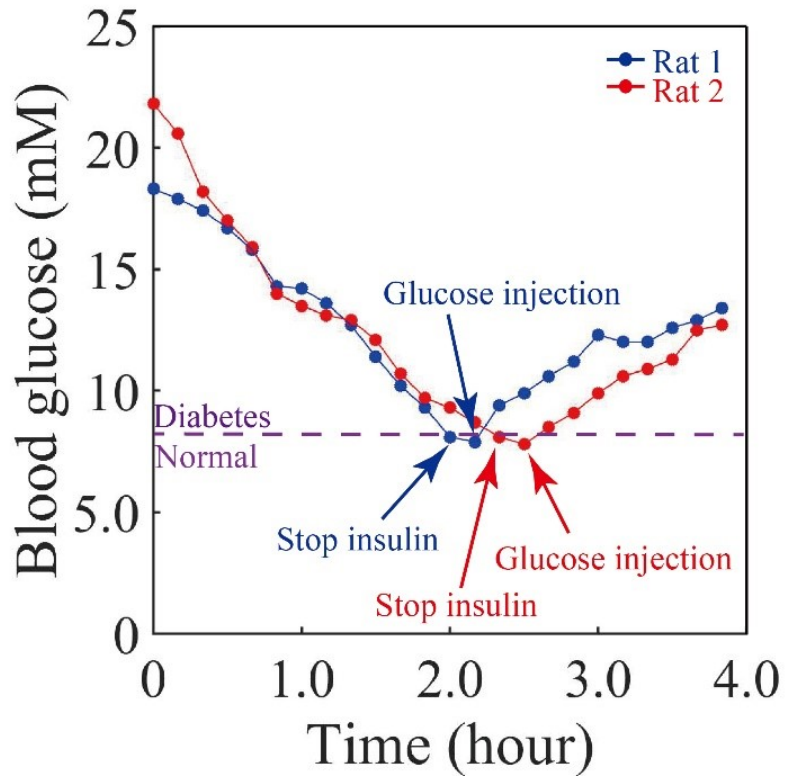


Fig. S29 The blood glucose levels versus time with the closed-loop button-like system in another two rats with the injection of glucose intraperitoneally.

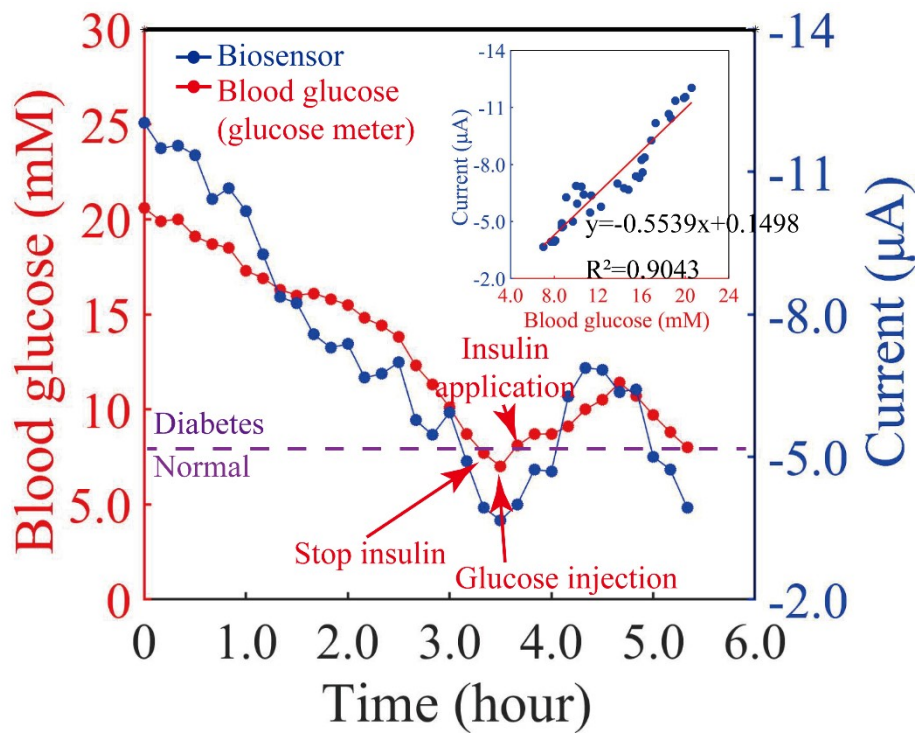


Fig. S30 The blood glucose levels versus time with the closed-loop button-like system with a glucose intake in a terminal-stage diabetic rat (the model time was one month ago).

Table S1. Comparison of this work and other micropumps in closed-loop management systems

Device	Working principle	Pump size	Insulin flow rate	Stability	Reference
Commercial 770G insulin pump developed by Medtronic Inc.	Electro-motor	9×6×2 cm	Automatically adjust insulin delivery rate every 5 minutes with the accuracy of 0.025 U/h	Stable for long-term	1
Iontophoresis with microneedle array	Iontophoresis	About 4.3 cm ²	5 IU released into the body in 3 hours	No stability evaluation	2
3D printed syringe with microneedle array	Syringe	Large size	No precise release rate	No stability evaluation	3
Electroosmotic pump with microneedle array	Electroosmotic	2.5 cm in diameter and 1.5 cm in thickness	Maximum flow rate: 9.42 μl/min for 10 U/ml insulin	Flow rate decrease with time	4
Electroosmotic pump with microtube	Electroosmotic	2 cm in diameter and 1.5 cm in height	Maximum flow rate: 3.376 μl/min for 10 U/ml insulin	Flow rate decrease with time	5
Electrochemical pump with microneedle array	Electrolysis of water to generate gas bubbles for driving liquid motion	2 cm in diameter and 1.2 cm in height	Maximum flow rate: 22 μl/min for insulin and the flow rate does not change with the concentration of insulin	Stable for 14 days	This work

References

1. Medtronic, The MiniMed™ 770G System, <https://www.medtronicdiabetes.com/products/minimed-770g-insulin-pump-system#prod-comparison>).
2. X. L. Li, X. S. Huang, J. S. Mo, H. Wang, Q. Q. Huang, C. Yang, T. Zhang, H. J. Chen, T. Hang, F. M. Liu, L. L. Jiang, Q. N. Wu, H. B. Li, N. Hu and X. Xie, *Adv. Sci.*, 2021, **8**, 2100827.
3. O. Heifler, E. Borberg, N. Harpak, M. Zverzhinetsky, V. Krivitsky, I. Gabriel, V. Fourman, D. Sherman and F. Patolsky, *ACS Nano*, 2021, **15**, 12019-12033.
4. X. J. Luo, Q. Yu, Y. Q. Liu, W. X. Gai, L. Ye, L. Yang and Y. Cui, *ACS Sens.*, 2022, **7**, 1347-1360.
5. Y. Q. Liu, Q. Yu, X. J. Luo, L. Ye, L. Yang and Y. Cui, *Research*, 2022, **Article in press**, 9870637.